Solar and Ionospheric Plasmas in the Ring Current Region

T. E. Moore[1], M-C. Fok[1], M. O. Chandler[2], S.-H. Chen[1], S. P. Christon[1], D. C. Delcourt[3], J. Fedder[4], M. Liemohn[5], W. K. Peterson[6], S. Slinker[7]

1. NASA's Goddard Space Flight Center, Greenbelt, MD USA; 2. NSSTC, NASA Marshall Space Flight Center, Huntsville, AL USA; 3. CETP, St. Maur, France; 4. George Mason Univ., Vienna, VA USA; 5. University of Michigan, Ann Arbor, MI USA; 6. University of Colorado, Boulder, CO USA; 7. Naval Research Laboratory, Washington, DC USA.

Submitted to proceedings of the Yosemite Workshop on Magnetospheric Imaging, June 2004

Abstract

We consider formation of ring current-like plasmas in the inner magnetosphere and explore the degree to which they derive from heating and outflow of ionospheric plasmas. Recent observations show ring current proton injection into the ring current is relatively smooth and continuous, while O^+ injection is episodic in close association with substorms. We use collisionless test particle motions in magnetospheric fields from a magnetohydrodynamic simulation. The simulation is used to generate bulk properties and detailed velocity distributions at key locations, for comparison with observations. Particles are initiated in regions representative of the solar wind proton source upstream of the bow shock, the polar wind proton source, and the auroral zone enhanced outflows of O^+, which we term "auroral wind". Results reflect steady growth phase conditions after 45 minutes of southward interplanetary field. Solar wind protons enter the ring current principally via the dawn flank, bypassing the midnight plasma sheet, while polar wind protons and auroral wind O^+ enter the ring current through the midnight plasma sheet. Thus, solar wind and ionospheric plasmas take very different transport paths to the ring current region. Accordingly, they are expected to respond differently to substorm dynamics of the magnetotail, as observed recently by remote neutral atom imaging from the IMAGE mission. Polar wind protons make a minor contribution to ring current pressure under steady conditions, but auroral wind O^+ has the potential to dominate the ring current, when outflow is strongly enhanced during periods of enhanced solar wind dynamic pressure fluctuations.

Introduction

Since the definitive observation of geogenic (O^+) ions in the magnetosphere [Shelley et al., 1973], it has been known that ionospheric cold plasmas contribute to the hot plasmas of the magnetosphere. But it was also observed that heavy ions are an important constituent during times of magnetospheric storms, when there is substantial dissipation of energy in the ionosphere proper, below a few thousand km altitude [Peterson et al., 1981, 1982; Sharp et al., 1985; Hamilton et al., 1988; Daglis et al., 1999]. Observations have gradually revealed that energy dissipated in the ionosphere goes partly into energization of heavy ions sufficient to overcome their gravitational binding to the Earth [beginning with Sharp et al., 1976; Klumpar et al., 1979]. A review of the ionospheric supply of magnetospheric plasma sources was given by Moore et al., [1999a]. More recent trajectory work by Cully et al. [2003] shows that the ionospheric supply of plasma to the plasma sheet, especially heavy O^+ plasma, is not only important but is strongly modulated by convection as driven by the interplanetary magnetic field. Moreover, the O^+ in the energetic ring current has been observed to be much more strongly modulated by substorm dynamics than the proton component [Mitchell, 2003].

The ionosphere has been known to supply cold light ion plasma to the magnetosphere since the discovery of the plasmasphere [Freeman et al., 1977]. On openly convecting field lines, polar wind flows continuously as convection opens the field lines and empties their accumulations into the polar lobes and downstream solar wind, so that they never reach equilibrium pressures. Dense plasmapheric plasmas result from polar wind-like light ion outflows into the nearly co-rotating inner magnetosphere, where they are trapped and accumulate to equilibrium pressures, and are therefore called “refilling flows.” Recently, the outer plasmasphere has been shown to flow sunward during magnetospheric disturbances [Elphic et al., 1997; Sandel et al., 2001; Goldstein et al., 2002]. The roots of plasmaspheric plume flux tubes create a corresponding plume of enhanced plasma density in the ionosphere proper [Foster et al., 2002]. Moreover, these cold plasmas have been discovered to be present in the subsolar low latitude magnetopause region under a wide variety of conditions [Su et al., 2001; Chandler and Moore, 2003; Chen and Moore, 2004]. When strong convection drains away part of the plasmasphere, the supply of plasma is enhanced in a transient way by the rapid release of accumulated plasma. Under steady conditions, however, the plasmasphere remains trapped and the magnetosphere is supplied only from the higher latitude polar wind outflow regions.

The contribution of ionospheric light ions to magnetospheric hot plasmas is less well established and is complicated by the difficulty of discriminating protons of solar or geogenic origin. Christon et al. [1994] used energy spectral features, in comparison with He^{++} assumed to be of solar origin, to estimate the relative contributions. They found that both solar wind and polar wind contributed comparable densities to the hot magnetospheric plasmas, with a somewhat greater ionospheric contribution for high solar activity levels.

In this paper we simulate the entry of solar wind plasmas into the inner magnetosphere under growth phase conditions of southward interplanetary field. We also consider the light ion polar wind outflows that are pervasive, continuous, and at most weakly responsive to solar wind intensity or magnetospheric activity. Finally, we consider the outflow of heavy ions from the active auroral zones, associated with electromagnetic and kinetic energy dissipation within the ionosphere proper, referring to the latter as “auroral wind”. We defer consideration of more typical “Parker spiral” IMF with By dominant. Light ion auroral outflows have fluxes similar to polar wind, while the heavy ion outflows have fluxes that range from much less than to much greater than polar wind outflows depending on the free energy available [Moore et al., 1999b]. Using these simulations, we address the question of how solar and polar wind protons, and auroral wind oxygen ions, are distributed in the magnetosphere during conditions that lead toward storm time ring current development.

Observations

We begin by presenting, in Figure 1, velocity distribution observations from the Polar spacecraft, the orbital apogee of which reached to the equatorial plasma sheet at 9-10 Re and swung through the midnight region during the Fall of 2001, and 2002. The plasma sheet is highly dynamic on time scales that cannot be sampled continuously using the 18 hour orbit of Polar. In the present paper, we focus instead on the persistent structure of this region and the ion velocity distributions that define that structure in relatively quiet times, but we also point toward variations that would be expected during more active periods.

A pervasive feature of the Polar observations in this region is the existence of cold high Mach number field-aligned flows away from the Earth in the lobe regions. We term these “lobal wind”, defining them as a mixture of polar wind and dayside auroral winds from the cleft ion fountain region. A second pervasive feature is the hot and therefore low Mach number flow of ions, embedded within the colder lobal wind outflows. These are identified as nightside auroral wind outflows of either the beam or conic varieties, depending on the ratio of perpendicular to parallel thermal speed. These appear with varying prominence, presumably dependent upon the conjugate auroral activity at the point of observation. They have higher parallel and perpendicular energy, with a broader angular pattern, than the relatively cold lobal wind flows. While the range of energies is continuous, such auroral outflows are usually distinguished from the lobal wind flows within which they are embedded.

Figure 1 summarizes these observations schematically, showing the various velocity distribution types in their typical arrangement along a Polar orbit, relative to the current sheet, plasma sheet, and lobes. The plasma sheet appears as a layered structure of velocity distribution features, as described above. There is considerable variability in the extent and prominence of the various features from pass to pass, presumably associated with convection and auroral activity. A substantial repeatability of this pattern is observed over many passes through the region, and it can be considered as an underlying structure, upon which variations are superposed. In the following sections, we investigate the degree to which this structure can be understood in terms of the particle populations that enter and travel through the plasma sheet region.

Figure 1. A schematic collage of the velocity distribution types and their association with observing position relative to the current sheet, along a typical Polar Orbit during Fall 2001-2002.

Motivation for considering the contributions of polar and auroral winds to the ring current has been found in recent observations from the IMAGE mission. In Figure 2, we reproduce an illustration of the compositional variability of the ring current, from Mitchell et al. [2003]. The main point of this study is that ring current oxygen ions are strongly modulated by substorm activity, while the lighter protons are less influenced by individual substorms, appearing to respond primarily on longer time scales to the storm growth phase. A possible interpretation of this observation is that O^+ injection to the ring current is relatively direct and driven by individual substorms while proton injections are related to larger scale magnetospheric phenomena such as global convection. Another related hypothesis is that substorm energization mechanisms are more effective on higher mass species. Here, we focus on global convection and transport simulations, rather than substorm dynamics. However, our results will turn out to have implications for this observation.

Figure 2. Variation of H+ and O+ ring current fluxes in association with substorms as documented by auroral imagery [after Mitchell et al., 2003].

Intimately related to the injection of new plasmas from the nightside plasma sheet, into the ring current region, is the stripping away of the outer plasmaspheric plasmas to form a cold plasma plume. This in turn is transported sunward toward the magnetopause [Goldstein et al., 2003]. In Figure 3, we exhibit recent observations that clearly reveal the arrival of those plasmas in the subsolar magnetopause region [Chandler and Moore, 2003]. It is clear that these plasmas flow into subsolar reconnection regions and are entrained into the downstream flows of the low latitude boundary layer and high latitude mantle [Chen and Moore, 2004]. They thus provide a source of relatively slow ions that may later be recycled into the flows returning through the inner magnetosphere, serving as a delayed source of the ring current, to the degree that they are energized by the process. In this process the dominant light ions may be expected to mimic the behavior of entering solar wind protons.

Figure 3. Observations of plasmaspheric plume formation (upper panel after Sandel et al. [2001], and of the presence of plasmaspheric plasma at the dayside magnetopause (lower panel, after Chandler and Moore [2003].

Our objective in what follows is to contribute toward understanding of the ionospheric plasma circulation cycle, driven by its contact with the solar wind flows. We seek to describe the nature of solar wind proton flows around and through the magnetospheric system, to accomplish the same for polar wind and auroral wind flows, and then to develop a basis for comment on observations of detailed velocity distributions and of substorm variations within storms. These will serve as a basis to plan further studies involving dynamic fields during the growth phase of storms.

Modeling

For this study, we implemented a 3D full particle motion calculation in fields that are specified on a regular spatial grid of points to accept field prescriptions from dynamic models. This calculation is based on the full particle simulation of Delcourt et al. [1993]. The particles are propagated in self-consistently computed fields from the magnetohydrodynamic simulation of Lyon, Fedder, and Mobarry [Fedder et al., 1995; Mobarry et al., 1996]. The advantage of using MHD fields is that we can consider the entry of solar wind through realistic boundary layer fields with reconnection operative in at least a qualitatively realistic way. Ionospheric outflows were not included in this calculation, but the F region ionosphere is modeled so that there is drag on the system at the roots of the flux tubes, represented by field-aligned current systems and ionospheric conductivity. For computational efficiency, we resampled the LFM fields onto a spherical grid with polar axis aligned to the GSM-X axis. The spacing in polar angle is a uniform 2˚ and the resolution in azimuthal angle on the GSM XY plane is ~5.5 deg. The grid spacing in radius varies with polar and azimuth angles with higher spatial resolution on the dayside and lower on the nightside. This approach allows very rapid identification of the current cell in which a particle is positioned, as it moves, conserving computing resources.

Interpolation between the grid points of the MHD simulation enables calculation of field values at any point, as a particle moves about within the simulation space. This is accomplished by simple linear interpolation in place of more sophisticated techniques that would allow continuous field gradients at the grid points. The inevitable field gradient discontinuities at grid points are a source of numerical diffusion, decreasing with the spacing of the grid used.

We step the particles in time many cycles per gyro period, typically 72 times or every 5 deg. of gyrophase, using Delcourt's double precision implementation of a 4^{th} order Runge-Kutta algorithm. We have previously shown [Moore et al., 2001], that the trajectories are precisely reversible over flight paths of many 10s of R_E, and many hours (when used with analytically continuous fields).

Our results are sensitive to grid and temporal spacing, indicating numerical errors. To minimize such effects, we used the finest practical grid spacing for our MHD simulation fields, and determined that the numerical effects were substantially reduced. The main effect of such errors is a diffusive effect on the particle trajectories that mimics real field variability, but is not currently guided by observed field fluctuations. We plan to introduce observed or simulated field fluctuations and reduce numerical effects to a comparatively negligible level, as soon as practicable.

For the solar wind, initial positions were randomly selected from a uniform distribution over the GSM YZ plane at Xgsm = 15 R_E, upstream of the simulated bow shock. For the polar wind, we started protons at 4 R_E altitude with invariant latitudes randomly distributed above 55˚ and over all local times. Auroral acceleration processes have not been applied to polar wind protons originating from that region. Though the total escaping flux of protons is relatively unaffected by such processes [Moore et al., 1999a], the circulation of protons accelerated by auroral processes will be more like that of O^+ ions treated as accelerated nightside auroral wind. For the auroral wind, we started O^+ at 1000 km altitude within a nominal auroral oval that was divided into dayside and nightside parts along the dawn-dusk meridian, as described in Table 1. Initial velocities were selected randomly from a uniform distribution of boxcar width equal to the specified bulk and thermal speeds, as shown in Table 1. Particles were run until they precipitated into the atmosphere, escaped from the simulation volume, or exceeded a time limit of 10-24 hours to assure that each particle makes at least one circumnavigation of the Earth, regardless of energy. A given particle contributes to a given cell only upon its first entry into that cell. Subsequent returns to the same cell are ignored.

Table 1. Source region particle initial conditions

Parameter	Value	Comment
Solar Wind		

Density	6.5 cm-3	typical
Thermal speed (Temp)	31 km/s (5 eV)	“
Velocity	400 km/s	“
Flux	3 x 10^8 $cm^{-2}s^{-1}$	
Polar Wind		
Density	0.5 cm-3	Su et al., 1998
Thermal speed (Temp)	17 km/s (1.5 eV)	“
Velocity	100 km/s	“
Flux	3 x 10^8 $cm^{-2}s^{-1}$	“
Auroral Wind O^+ (day)		75˚ to 65˚ ILat range
Density	1000 cm-3	Pollock et al., 1990
Thermal speed (Temp)	10 km/s (10 eV)	“
Velocity	10 km/s	“
Flux	1 x 10^9 $cm^{-2}s^{-1}$	“
Auroral Wind O^+ (night)		75˚ to 60˚ ILat range
Density	10 cm-3	Yau et al., 1988
Thermal speed (Temp)	100 km/s (1000 eV)	“
Velocity	100 km/s	“
Flux	1 x 10^8 $cm^{-2}s^{-1}$	“

A large number of particle trajectories was run and accumulated into a database of bins with resolution of 1 R_E^3, for all particles. The record for each particle consists of one record describing the particle initial conditions, and many records describing the particle state as it crosses each boundary in physical space. Entry and exit times are recorded as particles transition between cells, providing a time of flight through each cell. Particles were run with randomly selected initial conditions (within specified ranges) until the most populated bins contained >1000 particles. Some bins tend to remain empty, particularly for solar particles, because most of them pass through the system without entering the magnetosphere. To counter this, additional solar particles were run, focusing on the upstream regions with the highest probability of entry, until the most populated inner magnetosphere bins contained >100 solar particles. Requiring 100 particles in each bin provides reasonable statistical errors (<10%) for assessing the dominant transport paths, the shape of the particle velocity distribution, and for bulk properties of the plasma.

Bulk properties were estimated following an extension of the method described by Chappell et al. [1987] and Delcourt et al., [1989]. Examples of both are exhibited in subsequent figures. For each particle in a given spatial bin, the particle velocity and transit time for that bin are calculated. For a particle (i) passing through a particular bin (j), the contribution of density in this bin by this particle is:

$$nij = Fi * Tij / Vj \quad (1)$$

where Fi is the ion source flux in ion/s for particles of the specified velocity, Tij is the residence time of particle i in bin j, and Vj is the volume of bin j, that is 1 R_E^3 in our case.

Fi is specified directly by means of the density and flow of the source plasma across the source boundary.

$$Fi = ns * vs * dA \;;\; dA = A/NT \quad (2)$$

Here dA is the area of the source surface allocated to each particle, which is the total area of the source divided by the number of particles emitted, assuming a uniform distribution of particle emission on the source surface, which is must be assured when randomizing the initial locations. The source number density and flow velocity may be specified, or the product of those two is just as useful, if better known.

Substituting (2) into (1), we have

$$nij = ns * vs * A * Tij / (Vj * NT) \quad (3)$$

The density at bin j is just the summation of nij over all particles that are passing through bin j:

nj = Summation in i (nij) (4)

These relations can be applied to any source flowing across a boundary surface. The density from the ionospheric outflow can be calculated in a similar way. In that case, Vsw should by replaced by Vpw or Vaw and other parameters are replaced with values appropriate to the polar wind or auroral wind.

Once densities are calculated, the total (dynamic plus kinetic; we don't separate the two here) pressure at bin j is given by,

Pj = Summation in i (Pij) and

Pij = nij * Eij

where Eij is the average energy of particle i in bin j.

For the solar wind case:
ns = 5 cm-3; vs = 400 km/s or 4e7 cm/s; A = 3600 R_E^2; NT = 800000

For the polar wind case:
ns * vs = 3e8 $(1.15/4)^3$ $cm^{-2}s^{-1}$ = 7.1e6 $cm^{-2}s^{-1}$; A = area of sphere 4 Re radius for invariant latitudes above 55 deg; NT = 20000

For the auroral wind dayside case:
ns * vs = 1e9 $cm^{-2}s^{-1}$; A = area of sphere 1.15 Re within specified auroral oval; NT = 20000

For the auroral wind nightside case:
ns * vs = 1e8 $cm^{-2}s^{-1}$; A = area of sphere 1.15 Re within specified auroral oval; NT = 20000

This method distributes the source weighting properly with the number of particles emitted from any particular part of the boundary so that the results are unaffected by the number of trajectories initiated. This allows us, for example, to concentrate solar wind particles in the region with maximum probability of entry (subsolar), while using a smaller number of particles to define the magnetosheath flow.

The method also allows for the diffusive filling of velocity space from source populations that become highly structured in velocity space at some spatial locations [Moore et al., 2000]. If the relatively low resolution fields we use were realistic on all spatiotemporal scales, and there were no diffusive processes present, observed velocity distributions would be very finely structured with narrow features. In practice, magnetospheric fields include fluctuations over a wide range of frequencies, which are evidently diffusive, since extremely fine features are not observed within hot plasmas, though of course certain anisotropies are observed, as discussed above. Our bulk properties calculation attributes to each particle both a mean phase space density and a velocity space volume over which each particle is representative of the source. This allows for the particle weighting to be spread over the full region of velocity space at each location in the simulation space, rather than characterizing only a single point in velocity space.

The MHD fields for these simulations come from a time sequence that involves a few hours of northward Bz, an abrupt southward turning for two hours, and finally, a return to northward IMF [Slinker et al. 1995]. We selected a time about 45 minutes after the southward turning, well after the formation of a distant reconnection X line, but before the appearance of a near-Earth X line and ejection of a plasmoid. That is, we chose a state representative of the substorm growth phase, when the magnetotail closely resembles a Level-2 T89 field (corresponding to Kp ~ 1-2) earthward of the distant neutral line at ~40 R_E.

In Figure 4, the field snapshot is visualized in the XY and XZ planes. For the SBz case, subsolar reconnection and distant plasma sheet reconnection are both present, but are not in balance, and the plasma sheet is growing. Subsolar reconnection drives a high latitude flow that reinforces and becomes part of the double cell circulation flow in the equatorial plane. The magnetotail pressure distribution drives an earthward flow up to about 150 km/s in the inner

plasma sheet and especially along the flanks. The action of the distant neutral line helps to inflate the plasma sheet during this period, but it is being convected tailward and has relatively little influence on driving sunward convection at this point in the growth phase.

Figure 4. The computed magnetohydrodynamic fields for the SBz case. (top) The magnetic (B) lines are indicated in the noon-midnight meridian. (bottom) The electric field is indicated as color contoured values of the Vx in the GSM-XY plane, coded to discriminate sunward (reddish) from tailward (bluish) flows, with green indicating regions of relatively low velocity flows.

Results

In Figure 5 we display the plasma pressure in the GSM-XZ or noon-midnight meridian plane for the three sets of particles: solar wind, polar wind, and auroral wind. The bow shock and magnetosheath are prominent features, as are the cusps and the cross section of the inner ring current-like region. Solar wind protons tend to avoid the lobes and plasma sheet Earthward of -40 R_E, and it is unclear, from this view, how they are reaching the plasma sheet and the inner magnetosphere to form the ring current-like structure, where pressure of these protons reaches about 1-10 nPa. A clear plasma mantle has formed, from the lowest energy solar wind particles, which meet at the plasma sheet beyond 30-50 Re.

The polar wind outflow fills the lobes, some of it reaching the plasma sheet Earthward of about -40 Re and thence convecting back toward the Earth to form a region of drifting ring current-like protons that has a pressure of < 0.1 nPa. Polar wind protons are also seen to convect to the magnetopause where they are jetted up over the poles, participating in the magnetosheath flow as they escape downstream with a low partial pressure.

The auroral wind flows through the polar lobes (dayside part) or directly into the plasma sheet (nightside part), and reaches the plasma sheet earthward of about 25 Re. Most of this auroral wind flows sunward through the inner magnetosphere, forming a ring current population. It continues sunward to the magnetopause where it is entrained into the mantle and polar cap flows again, but this time at higher energy than when initially leaving the ionosphere. Consequently, it travels substantially farther down tail, in part beyond the limit at 70 Re in the simulation space, and in part returning Earthward through the plasma sheet a second time. The ring current region contains contributions from both first and second pass O^+ ions from the auroral wind, the latter being substantially more energetic, but less numerous.

Figure 5. Plasma pressure is color contoured in the GSM-XZ or noon-midnight meridian plane. Solar wind particle pressures are shown in the upper panel; polar wind particle pressures are shown in the middle panel; and auroral wind pressures are shown in the lower panel.

In Figure 6, we display the plasma pressure in the XY or ecliptic-equatorial plane, comparing solar wind, polar wind, and auroral wind contributions in the three panels. Features of interest for the solar wind include the bow shock, the magnetosheath, and the low latitude boundary layer flows, and formation of a cavity in the wake region, within which few trajectories penetrate, while those that do have a relatively low associated pressure compared with the solar wind proper. This probably reflects a requirement for entering solar wind ions to be of relatively low energy to convect to the neutral sheet before their parallel motion causes them to escape the system. The figure (with overlaid path/arrow) clearly reveals the principal path along which solar wind protons enter the inner magnetosphere, through the magnetopause along the dawn flank, then looping back to form a drifting ring current-like population, with a pressure reaching >1 nPa. This feature is not as close to Earth as a full storm-time ring current, reflecting relatively weak inner magnetospheric convection. This owes in part to the moderate SBz conditions for this simulation.

Polar wind ions populate the plasma sheet, escaping downstream where they land beyond the convection reversal of Figure 5, and returning Earthward where they land within the Earthward flow. The latter illuminate a clear plasma sheet structure that connects directly with the inner magnetospheric closed drift region. Ionospheric plasma that is convected to the sunward magnetopause region is then entrained into the inner magnetosheath along flanks of the magnetosphere and downstream as part of the low latitude boundary layer.

The auroral wind behaves similarly to the polar wind in this view, but with substantially greater pressure contribution, especially in the inner magnetospheric ring current region, where pressure reaches 10's of nPa for the outflow fluxes assumed here. In addition, there is a larger dawn dusk asymmetry of both the plasma sheet and ring current pressure distributions for the auroral wind. Substantial downstream plumes are formed in the low latitude boundary layers here as in the polar wind case.

Figure 6. The plasma pressure is color contoured in the GSM-XY or equatorial plane. Solar wind particle pressures are shown in the upper panel; polar wind particle pressures are shown in the middle panel; and auroral wind pressure in the lower panel.

In Figure 7, we display the plasma pressure in the last of the three cardinal planes, the GSM-YZ plane at X = 0, or the dawn-dusk meridian. This cross section is dominated by solar wind and magnetosheath flows. The magnetospheric lobes are prominent in both solar wind and polar wind proton pressure, though for solar protons, they are profoundly empty at the core, but with a mantle of low energy solar protons as well.

The polar wind protons populates the lobes, but at relatively low pressure. The magnetosheath contains an enhancement of polar wind proton pressure, but it is still a minor addition to solar wind pressure. For the solar wind, a dawn-dusk asymmetry between the magnetosheath and the inner region hints at the dominant entry pattern into the inner magnetosphere via the dawn flank, but the view of this is better in Figure 6.

The auroral wind O^+ also shows the dawn-dusk asymmetry seen earlier in the XY plane, which extends into the lobes, where it has the opposite sense as in the inner magnetosphere (and the same sense as in the plasma sheet. This presumably reflects circulation asymmetries in convection, combined with the recirculation of auroral wind outflows reaching the dayside magnetopause.

Figure 7. For the SBz case, the plasma pressure is color contoured in the GSM-YZ or dawn-dusk meridian plane. Solar wind particle pressures are shown in the upper panel; polar wind particle pressures are shown in the middle panel; and auroral wind pressures in the lower panel.

In Figure 8, we display an array of velocity distributions for solar, polar and auroral wind particles. In the upper row, angular integrations are used to derive energy distributions by density contribution. We find that the solar wind contribution contains components at around 1 keV and at about 40 keV. The polar wind, in contrast, yields a population dominated by the lowest energies around 100 eV, declining steeply into the 10's of keV. The auroral wind has a 10's eV component evidently deriving from direct outflow from the dayside region, and a dominant 10's keV component that exceeds all others.

In the middle row, the full (2D) velocity distributions are given with color coding according to density contribution (a normalized phase space density). Here we see angular structure mainly in the polar wind core particles, which have a pancake distribution in this region. In the auroral wind particles, field alignment is seen in the lowest energy population, which originates from the night side auroral zone outflows. Additional details indicate the density, pressure and average energy for these populations.

In the lower row of panels, the same velocity distributions are coded with a color indicating the maximum excursion of each particle from Earth during its history prior to arrival in this spatial bin. The main point here for solar wind particles is that the energetic component has generally entered the inner magnetosphere without exceeding their original distance of 15 Re upstream. The low energy component has evidently traveled farther downstream, and these are the low energy particles of the incident solar wind that formed the mantle flow. The polar wind has an opposite trend with the most energetic component having traveled farthest down the tail before returning, with a sprinkling of exceptional particles. The lowest energy core of the polar wind particles has evidently been locally emitted from the ionosphere without passing through the plasma sheet. For auroral wind particles, there is a similar mixture of local low energy core and energetic component that has traveled farther down tail, but then at the highest energies we again see that the origin becomes more local.

Figure 8. Velocity distributions at selected locations for the SBz fields case: a) for polar wind particles only from –2.5 ≤ Zgsm ≤ 2.5 at Ygsm = 0 and Xgsm = -30 Re; b) for polar wind and solar wind particles from –10< Zgms < 10

at Ygsm =0, Xgsm = -10 Re; c) for polar wind particles at Ygsm = 6 and Xgsm = Zgsm = 0; d) for solar wind particles at Ygsm=6, Xgsm = Zgsm = 0. Inset panels show the angle-integrated energy distribution of polar and solar wind protons. NOTE: the velocity scales vary from panel to panel in this figure.

In Figure 9, we display a pair of O^+ trajectories typical of dayside and nightside outflows, illustrating some of the points made above. In particular, the upper panels show a dayside O+ ion, launched near 11 MLT with an initial energy of 42 eV, and initially convected tailward through the polar lobe. As a consequence of its low energy, the ion is deflected dawnward as it arrives in the near-Earth plasma sheet and convects sunward. When it reaches the dayside cusp region, it again travels tailward through the lobe, this time at higher altitude, and traveling farther down tail. It is significantly accelerated upon traversing the neutral sheet and transported duskward. Its energy is then high enough to drift through the dusk sector toward the dayside magnetopause, where it is again sent tailward, but this time with too much energy to be captured in the tail, approximately 25 keV.

The lower panels of Figure 9 illustrate a nightside auroral O^+ ion, launched at about 2100 MLT with an initial energy of 2.4 keV. This is a high enough energy that the ion travels sunward through the dusk sector on its first pass. The ion misses the stretched part of the plasma sheet and gains no significant energy in its first pass. It reaches the dayside and is again carried tailward through the lobes, reaching the neutral sheet at about -45 R_E and gaining substantial energy as it swings across the neutra sheet and is then convected earthward, but swings wide toward the dusk flank, where it excapes into the downstream magnetosheath. The final energy is similar to that of the dayside outflow O^+ ion, but whereas the dayside auroral wind ion is retained in the inner magnetosphere, the nightside auroral ion drifts duskward and fails to make a second pass through the inner magnetosphere.

Figure 9. Example trajectories for the auroral wind O+ ions. The upper set of panels show three projections and the energy history for a dayside emitted auroral wind ion. The lower set of panels show three projections and the energy history for a nightside emitted auroral wind ion. Initial and final conditions are summarized in the inset text listings for each trajectory.

Summary Discussion

We have previously suggested [Moore et al., 2001] that much of the plasma sheet and ring current plasma may be provided by ionospheric sources, even though it is clear that the solar wind supplies the energy to power magnetospheric phenomena. Delcourt and Moore [1992] looked at solar wind entry and concluded that it was exceedingly difficult to get solar wind protons arriving via the dayside cusp region to reach the inner magnetosphere through the plasma sheet. We failed at that time to consider entry along the low latitude boundary layers near the flanks of the magnetosphere, but others have suggested or pointed out that entry path [Lennartsson, 1994; Richard, 2002, Walker, 2003, Peroomian, 2003, Winglee, 2003; Thomsen et al, 2003]. On the other hand, the polar wind contribution to the plasma sheet has not been studied as carefully as the solar wind since Hill [1975]. We have taken a more comprehensive approach to both solar wind entry and polar wind circulation than we did earlier, by initiating particles in the boundary regions and tracking them through a realistic interaction from MHD simulations [Moore et al., 2005]. To that we have now added the ionospheric source of O^+ from the auroral zones, both dayside and nightside, which we have termed “auroral wind”.

To explore both the transport paths and kinetic behaviors of the plasma ions, we treated them using single particle motions in global fields. The fields derive from a snapshot of magnetohydrodynamic simulations and are therefore realistic in terms of bulk plasma and electrodynamic parameters, but frozen in time during the particle motions. No diffusive effects were included, but particles were introduced with randomized gyrophase and suffer some diffusive numerical effects. The fields are based only on a solar wind plasma source, revealing an implicit assumption that the ionospheric plasma does not alter the dynamics of the MHD simulation. The magnetosphere was considered at equinox with no dipole tilt off normal to the Sun-Earth line. These limitations have been introduced to make this work practical. We believe them to have relatively minor impacts on the conclusions drawn from this work, but plan to explore the dynamic effects of polar and auroral winds in future work using similar or multifluid simulations.

In agreement with results of others cited above, we find that the dawn low latitude boundary layer region is the most effective source of solar wind particles to the ring current region. This route supplies the inner ring current region independent of the path through the midnight plasma sheet near the reconnection region and dominates over that path, which is much lower in solar proton density and pressure, compared with the dawn entry route, but is well-

populated with polar wind, which then flows into the ring current region along the traditional path. For the SBz conditions we studied, the solar wind contribution to the inner magnetospheric ring current region is dominant over the polar wind contribution in pressure and the two are comparable in density, with the solar wind energy distribution having a greater mean energy. This result supports the conclusions reached by Hill [1975].

The current results should be considered in the context of the geopause suggested by Moore and Delcourt [1995]. It is apparent that solar wind protons enjoy a special access route to the inner magnetosphere that is quite different from that taken by ionospheric outflows (with the possible exception of such outflows into the dawn flank region). This effect, which appears to result from magnetic gradient drifts of solar wind protons, leads to an effective "wormhole" or leak of solar protons from the dawn low latitude boundary layer to the ring current region. It produces considerable mixing of the two sources in the inner magnetosphere, for the conditions considered here and allows the solar wind plasma to dominate the interior ring current-like region.

In contrast with the solar wind, the auroral wind follows the polar wind path to the plasma sheet and ring current region, but has a substantially larger source flux and a lower velocity (dayside) or smaller convective separation (nightside) from the ring current region. As a result, the auroral wind is initially more confined to the inner magnetosphere and can for active conditions have a larger flux than the polar wind by an order of magnitude or more.

In contrast with the polar wind, the auroral wind remains slower, even after passage through the inner magnetosphere. When it reaches the dayside reconnection region, it subsequently acts more like solar wind mantle (slow) than solar wind core (fast). Therefore, it is convects to the plasma sheet a second time and is recirculated to the inner magnetosphere a second time, again raising its energy and pressure. Together these make for substantially greater pressure of O^+ in the inner magnetosphere. Auroral O^+ is energized to a greater degree by its interactions with the plasma sheet and magnetospheric convection, and is successively energized during two or more passes through the system. Being slower at given energy, the auroral wind must reach higher energies before it is fast enough to escape downstream in the boundary layers. The net affect appears to be that heavy ion auroral wind is energized and concentrated within the magnetosphere to a greater degree than polar wind, and can also exceed the pressure of the solar wind proton component.

Conclusions

Solar wind ions enter principally along the dawn flank, bifurcating into a component that continues down the dawn flank, and another component that convects immediately into the inner magnetosphere and into the ring current without passing through the midnight plasma sheet. Polar wind fills the plasma sheet proper and supplies a plasma pressure contribution that is appreciable but minor, for the conditions we've studied in the ring current region. The density contributions of solar and polar wind protons are comparable, but the solar wind protons have a substantially higher mean energy and dominate the proton pressure.

In contrast, auroral wind O^+ has the capability to form the dominant component of the ring current pressure, particularly under active conditions that drive substantial dayside outflows [Moore et al., 1999; Strangeway et al., 2000], which we have assumed to be present here. Moreover, the auroral wind follows the polar wind path to the ring current and is thus arguably subject to substorm effects as observed by Mitchell et al. [2003]. Relatively slow auroral wind heavy ions are uniquely capable of making multiple circuits around the global magnetospheric circulation flow, gaining energy from each cycle. This new finding suggests the possibility of cumulative effects on the ring current involving sustained magnetospheric convection, but needs additional investigation using a dynamic multifluid global simulation. Somewhat surprisingly, accelerated nightside auroral wind flows do not appear to contribute substantially to the ring current pressure here. Contributing factors include the following: we have assumed their flux to be substantially smaller; they do not initially travel as far down the tail; their greater initial energy means that they drift duskward and tend to escape downstream through the dusk side flank, rather than being recirculated through the inner magnetosphere.

Simulated velocity distribution features in the inner plasma sheet agree well with Polar observations of high Mach number lobal wind supply of the plasma sheet, with interpenetration of the polar wind streams from the two lobes and heating to form counterstreaming plasma sheet boundary layer populations and a hot isotropic central plasma

sheet population. In the region observed by Polar, a hot solar wind proton distribution is found to occupy the current sheet region. These protons are on closed drift paths encircling the Earth for these conditions and may be considered part of the outer ring current. In the ring current-like region, the energy distributions of polar wind and solar wind protons agree very well with the results from AMPTE/CCE shown by Christon et al [1994] and support their identification of a soft component of polar wind origins, and an energetic peaked component of solar wind origins. The principal observed features of the inner plasma sheet are thus formed naturally from a combination of cold lobal wind outflows, combined with solar wind proton entry through the dawn flank region.

For conditions of moderate activity, magnetospheric transport of ionospheric and solar wind ions is very different. The solar wind entry path is via the dawn flank and thence rather directly into the inner plasma sheet and ring current regions. Consequently, the solar proton ring current should be less affected by substorms and other magnetotail phenomena, while the auroral wind outflows are expected to depend greatly on such processes. Thus, the behavior observed recently by Mitchell et al. [2003], with strong substorm modulation of Oxygen fluxes in the ring current, but with relatively little modulation of proton fluxes, appears to follow from our results. However, to fully explore this will require trajectory simulations in dynamically evolving fields. Though this was beyond the scope of the current study, have developed the tools necessary for this and will report on it in the near future.

Acknowledgements

The authors acknowledge support from the NASA Polar Mission under UPN 370-08 ; from the NASA IMAGE Mission under UPN 370-28, and from the NASA Geospace Sciences Program under UPN 344-42-01 for the Terrestrial Plasma Energization investigation.

References

Chandler, M. O., and T. E. Moore, Observations of the geopause at the equatorial magnetopause: Density and temperature, GRL, SSC6, 15 Aug, 2003.

Chappell, C. R., T. E. Moore, and J. H. Waite, Jr., The ionosphere as a fully adequate source of plasma for the Earth's magnetosphere, J. Geophys. Res. 92, 5896, 1987.

Chen, S.-H., and T. E. Moore, Dayside flow bursts in the Earth's magnetosphere, JGR, 109(A3), p.A03214, 18 March 2004.

Christon, S. P., G. Gloeckler, D. C. Hamilton, and F. M. Ipavich, A method for estimating the solar wind H+ contribution to magnetospheric plasma, in Solar Terrestrial Energy Program, 5th COSPAR Colloquium, D. N. Baker, V.O. Patitashvili and M.J. Teague, Eds., Pergammon Press, New York, 1994.

Cully, C.M., E.F. Donovan, A.W. Yau, and H.J. Opgenoorth, Supply of thermal ionospheric ions to the central plasma sheet J. Geophys. Res, 108(A2), 1092, 2003.

Daglis, I. A., G. Kasotakis, E. T. Sarris, Y. Kamide, S. Livi, and B. Wilken, Variations in the ion composition during an intense magnetic storm and their consequences, Phys. Chem. Earth, 24, p.229, 1999.

Delcourt, D. C., C. R. Chappell, T. E. Moore, and J. H. Waite, Jr., A three dimensional numerical model of ionospheric plasma in the magnetosphere, J. Geophys. Res 94, 11,893, 1989.

Delcourt, D. C., T. E. Moore, J. A. Sauvaud, and C. R. Chappell, "Non-Adiabatic Transport Features in the Outer Cusp Region," J. Geophys. Res., 97(A11), 16,833-16,842, 1992.

Delcourt, D.C., J.A. Sauvaud, and T. E. Moore, Polar wind dynamics in the magnetotail, J. Geophys. Res., 98(A6), 9155, 1993.

Delcourt, D. C., T. E. Moore, and C. R. Chappell, "Contributions of Low-Energy Ionospheric Protons to the Plasma Sheet," J. Geophys. Res., 99(A4), 5681-5689, 1994.

Elphic, R. C., M. F. Thomsen, and J. E. Borovsky, The fate of the outer plasmasphere, Geophys. Res. Lett., 24, 365, 1997.

Fedder, J. A., J. G. Lyon, S. P. Slinker, and C. M. Mobarry, Topological structure of the magnetotail as a function of interplanetary magnetic field direction, J. *Geophys. Res*., 100, 3613-3621, 1995.

Foster, J., P. J. Erickson, A. J. Coster, J. Goldstein, and F. J. Rich, Ionospheric signatures of plasmaspheric tails, Geophys. Res. Lett., v.29(13), p.1623, 2 July 2002.

Freeman, J. W., Jr., H. K. Hills, T. W. Hill, P. H. Reiff, and D. A. Hardy, Heavy ion circulation in the Earth's magnetosphere, Geophys. Res. Lett., 4, 195, 1977.

Goldstein, J., *et al.,* IMF-driven Plasmasphere Erosion of 10 July 2000, *Geophys. Res. Lett.*, 30, doi:10.1029/2002GL016478, 2003.

Klumpar, D. M., 1979, Transversely accelerated ions: An ionospheric source of hot magnetospheric ions, J. Geophys. Res. 84, 4229.

Lennartsson, W, Tail lobe ion composition at energies of 0.1 to 16keV/e: Evidence for mass-dependent density gradients, J. Geophys. Res. 99(A2), p.2387, 1994.

Mitchell, D. G., Pontus C:Son Brandt, Edmond C. Roelof, Douglas C. Hamilton, Kyle C. Retterer, And Steven Mende, "Global Imaging Of O+ From Image/Hena," *Space Science Reviews* 0: 1–13, 2003.

Mobarry, C. M., J. A. Fedder, and J. G. Lyon, Equatorial plasma convection from global simulations of the Earth's magnetosphere, *J. Geophys. Res., 101*, 7859-7874, 1996.

Moore, T. E., and D.C. Delcourt, The Geopause, Revs. Geophys. 33(2), p. 175., 1995a.

Moore, T. E., R. Lundin, et al., "Source processes in the high latitude ionosphere", Space Sci. Revs., 88(1-2), p.7, 1999; Chapter 2 of "Magnetospheric Plasma Sources and Losses, ed. by B. Hultqvist and M. Oieroset, Kluwer, Dordrecht, Holland, 1999a.

Moore, T. E., W. K. Peterson, C. T. Russell, M. O. Chandler, M. R. Collier, H. L. Collin, P. D. Craven, R. Fitzenreiter, B. L. Giles, and C. J. Pollock, Ionospheric mass ejection in response to a CME, Geophys. Res. Lett., 26(15), pp. 2339-2342, 1999b.

Moore, T. E., B. L. Giles, D. C. Delcourt, and M.-C. Fok, The plasma sheet source groove, J. Atmos. Solar Terr. Phys., 62(6), p.505, 2000.

Moore, T.E., M.O. Chandler, M.-C. Fok, B.L. Giles, D.C. Delcourt, J.L. Horwitz, C.J. Pollock, Ring Currents and Internal Plasma Sources, Space Science Reviews, 95(1/2): 555-568, January, 2001.

Peterson, W. K., R.D. Sharp, E.G. Shelley, R.G. Johnson, and H. Balsiger, Energetic Ion Composition of the Plasma Sheet, J. Geophys. Res. 86, 761, 1981.

Peterson, W.K., E.G. Shelley, G. Haerendel, and G. Paschmann, Energetic Ion Composition in the Subsolar Magnetopause and Boundary Layer, J. Geophys. Res. 87, 2139, 1982.

Peroomian V., The influence of the interplanetary magnetic field on the entry of solar wind ions into the magnetosphere, Geophys. Res. Lett., 30 (7), 1407, doi: 10.1029/2002GL016627, 2003.

Richard, R. L., M. El-Alaoui, M. Ashour-Abdalla, and R. J. Walker, Interplanetary magnetic field control of the entry of solar energetic particles into the magnetosphere, *J. Geophys. Res.*, *107*(A8), 1184, 10.1029/2001JA000099, 2002.

Sandel, B. R., et al., Initial Results from the IMAGE Extreme Ultraviolet Imager, Geophys. Res. Lett., 28(8), p. 1439, April 2001.

Sharp, R. D., R. G. Johnson, and E. G. Shelley, 1977, Observation of an ionospheric acceleration mechanism producing energetic (keV) ions primarily normal to the geomagnetic field direction, J. Geophys. Res. 82(22), 3324.

Sharp, R. D., W. Lennartsson, and R. J. Strangeway, The ionospheric contribution to the plasma environment in near-earth space, Radio Sci. 20, 456, 1985.

Shelley, E. G., R. G. Johnson, and R. D. Sharp, 1972, Satellite observations of energetic heavy ions during a geomagnetic storm, J. Geophys. Res. 77, 6104.

Slinker, S. P., J. A. Fedder, J. G. Lyon, Plasmoid formation and evolution in a numerical simulation of a substorm, Geophys. Res. Lett., 22(7), 859-862, 10.1029/95GL00300, 1995.

Stern, D. P., The motion of a proton in the equatorial magnetosphere, *J. Geophys. Res., 80*, 595-599, 1975.

Strangeway, R. J., C. T. Russell, C. W. Carlson, J. P. McFadden, R. E. Ergun, M. Temerin, D. M. Klumpar, W. K. Peterson, T. E. Moore, Cusp Field-Aligned Currents and Ion Outflows, J. Geophys. Res. 105(A9), p.21129, 2000.

Su, Y.-J., J. L. Horwitz, T. E. Moore, M. O. Chandler, P. D. Craven, B. L. Giles, M. Hirahara, and C. J. Pollock, Polar wind survey with Thermal Ion Dynamics Experiment/Plasma Source Instrument suite aboard POLAR, J. Geophys. Res., 103, 29,305, 1998.

Su, Y.-J., J. E. Borovsky, M. F. Thomsen, N. Dubouloz, M. O. Chandler, T. E. Moore, and M. Bouhram, Plasmaspheric material on high-latitude open field lines, J. Geophys. Res., 106, 6085, 2001.

Thomsen, M. F., J. E. Borovsky, R. M. Skoug, and C. W. Smith, The delivery of cold, dense plasma sheet material into the near-earth region, J. Geophys. Res., 108(A4), doi: 10.1029/ 2002JA009544, 2003.

Tsyganenko, N. A., A magnetospheric magnetic field model with a warped tail current sheet, Planet. Space Sci. 37, p.5, 1989.

Volland, H., A model of the magnetospheric convection electric field, *J. Geophys. Res.*,*83*, 2695-2705, 1978.

Walker, R. J., M. Ashour-Abdalla, T. Ogino, V. Peroomian, and R. L. Richard, Modeling magnetospheric sources, in *Earth's Low-Latitude Boundary Layer*, *Geophys. Monogr. Ser.*, vol. 133, edited by P. Newell and T. Onsager, p. 33, 2003.

Winglee, R. M., Circulation of ionospheric and solar wind particle populations during extended southward interplanetary magnetic field, *J. Geophys. Res.,* Vol. 108, No. A10, 1385, 10.1029/2002JA009819, 2003.

Figure 1

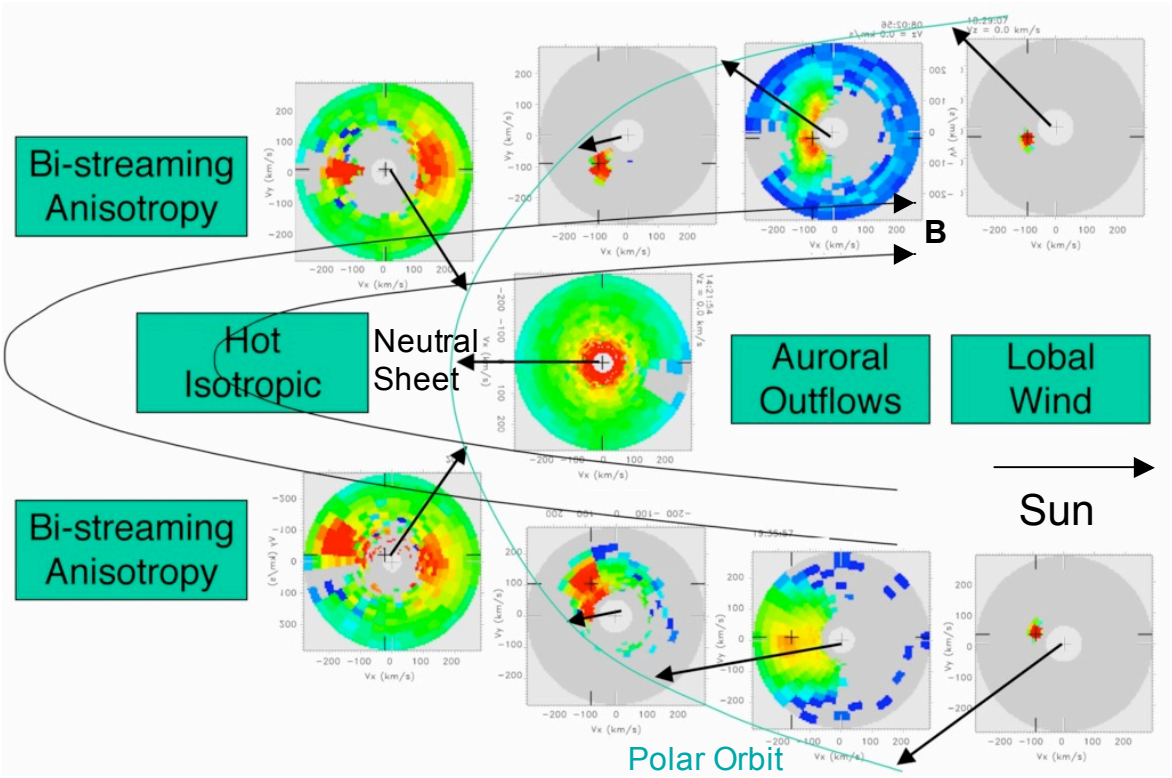
Bi-streaming Anisotropy
Hot Isotropic
Neutral Sheet
Auroral Outflows
Lobal Wind
Bi-streaming Anisotropy
B
Sun
Polar Orbit

Figure 2

IMAGE HENA and FUV 21 Oct 2001

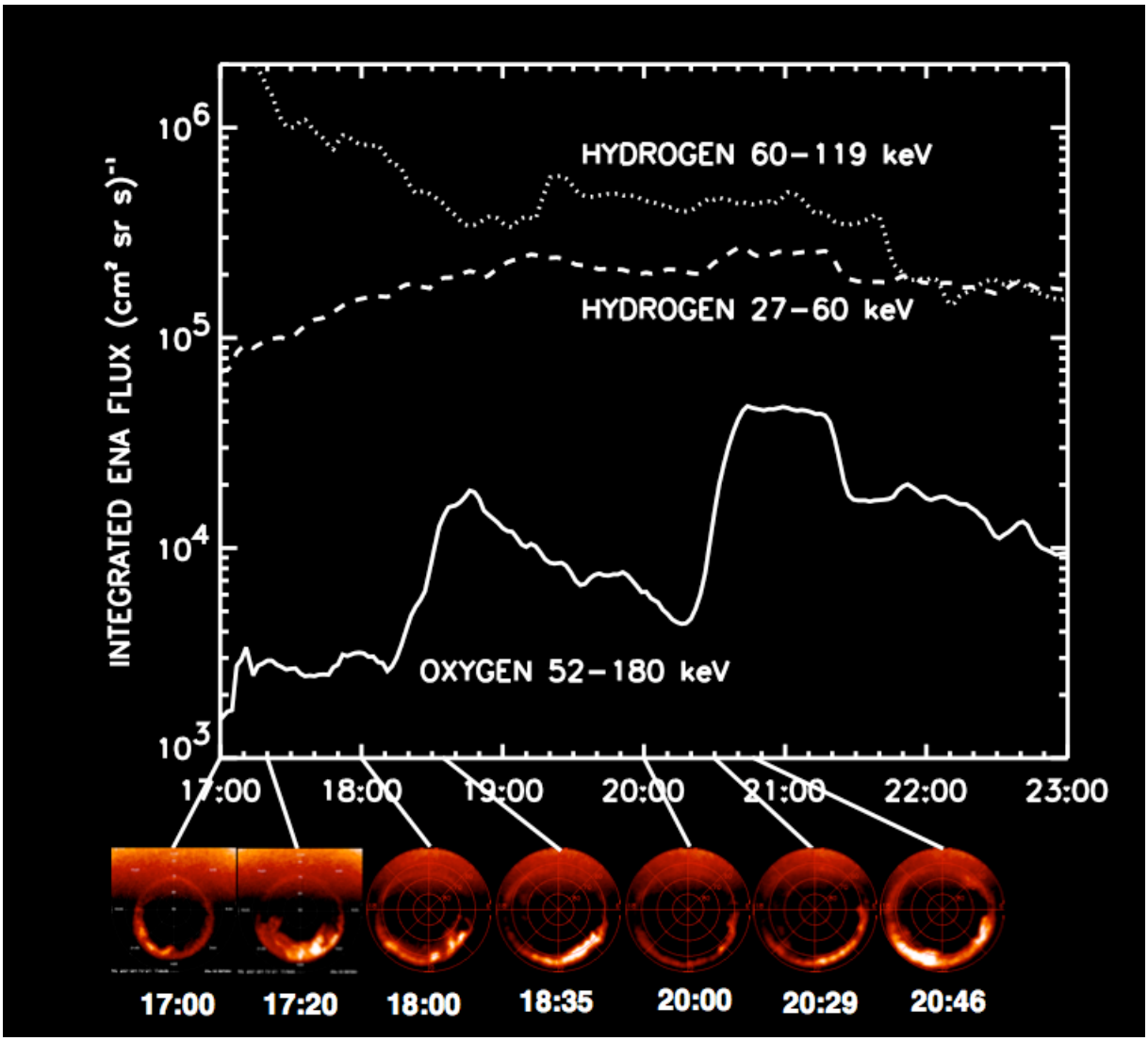

Figure 3

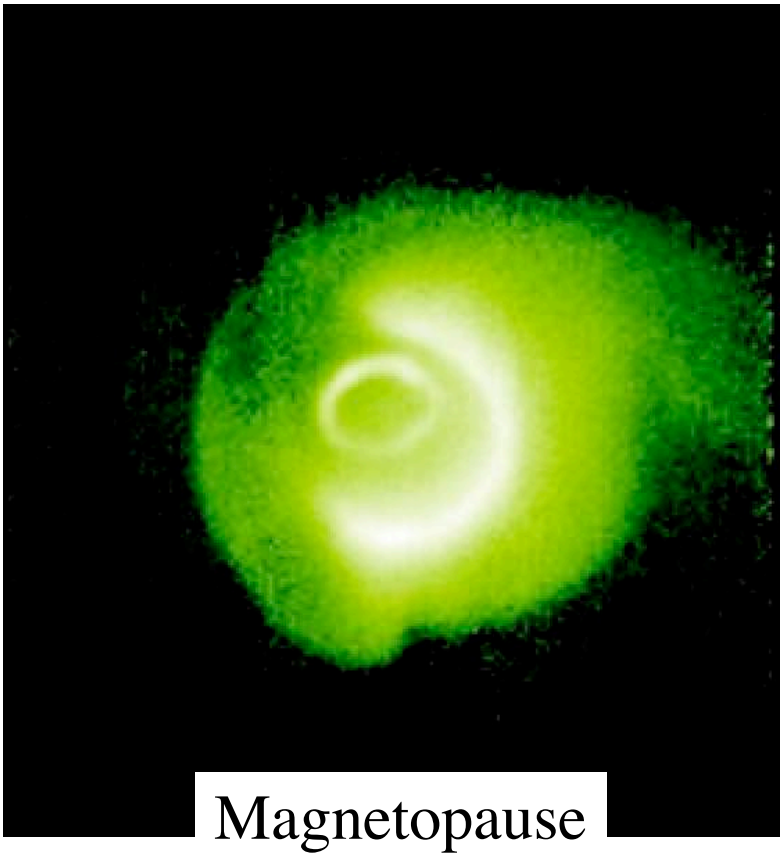
Magnetopause

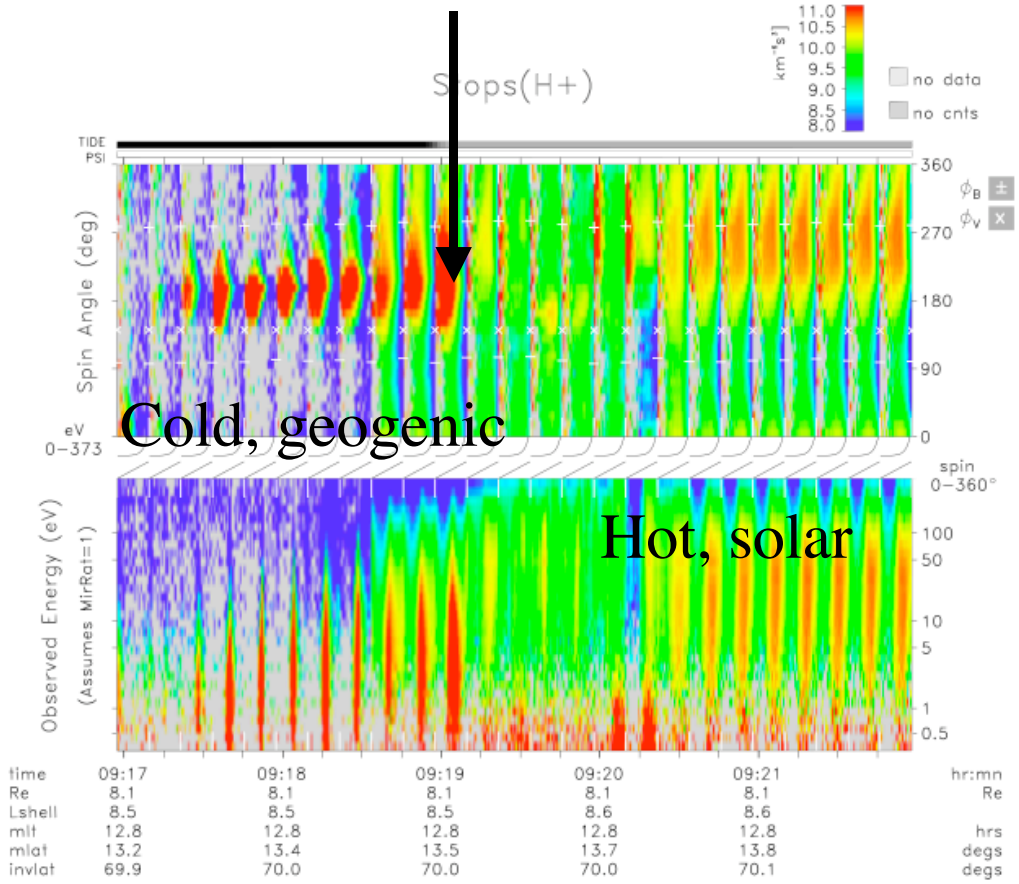
Stops(H+)
11.0
10.5
10.0
9.5
9.0
8.5
8.0
km*s/]
no data
no cnts
TIDE
PSI
Spin Angle (deg)
360
270
180
90
0
eV
0–373
Cold, geogenic
spin
0–360°
Observed Energy (eV)
(Assumes MirRat=1)
Hot, solar
100
50
10
5
1
0.5
time
Re
Lshell
mlt
mlat
invlat
09:17
09:18
09:19
09:20
09:21
8.1
8.5
12.8
13.2
69.9
13.4
70.0
13.5
13.7
13.8
70.1
hr:mn
hrs
degs
degs

Figure 4

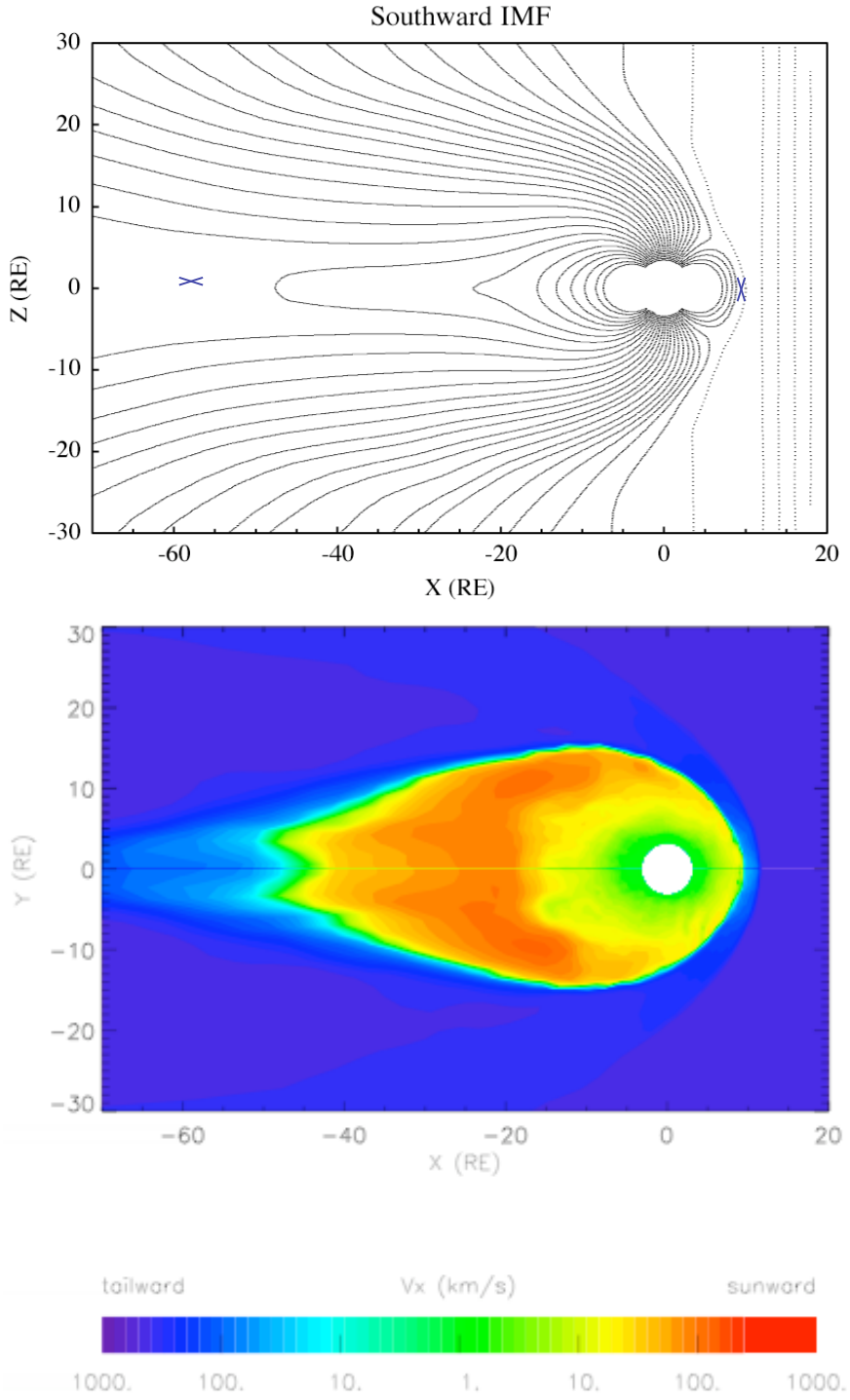
Southward IMF
Z (RE)
X (RE)
Y (RE)
X (RE)
tailward
Vx (km/s)
sunward
1000.
100.
10.
1.
10.
100.
1000.

Figure 5

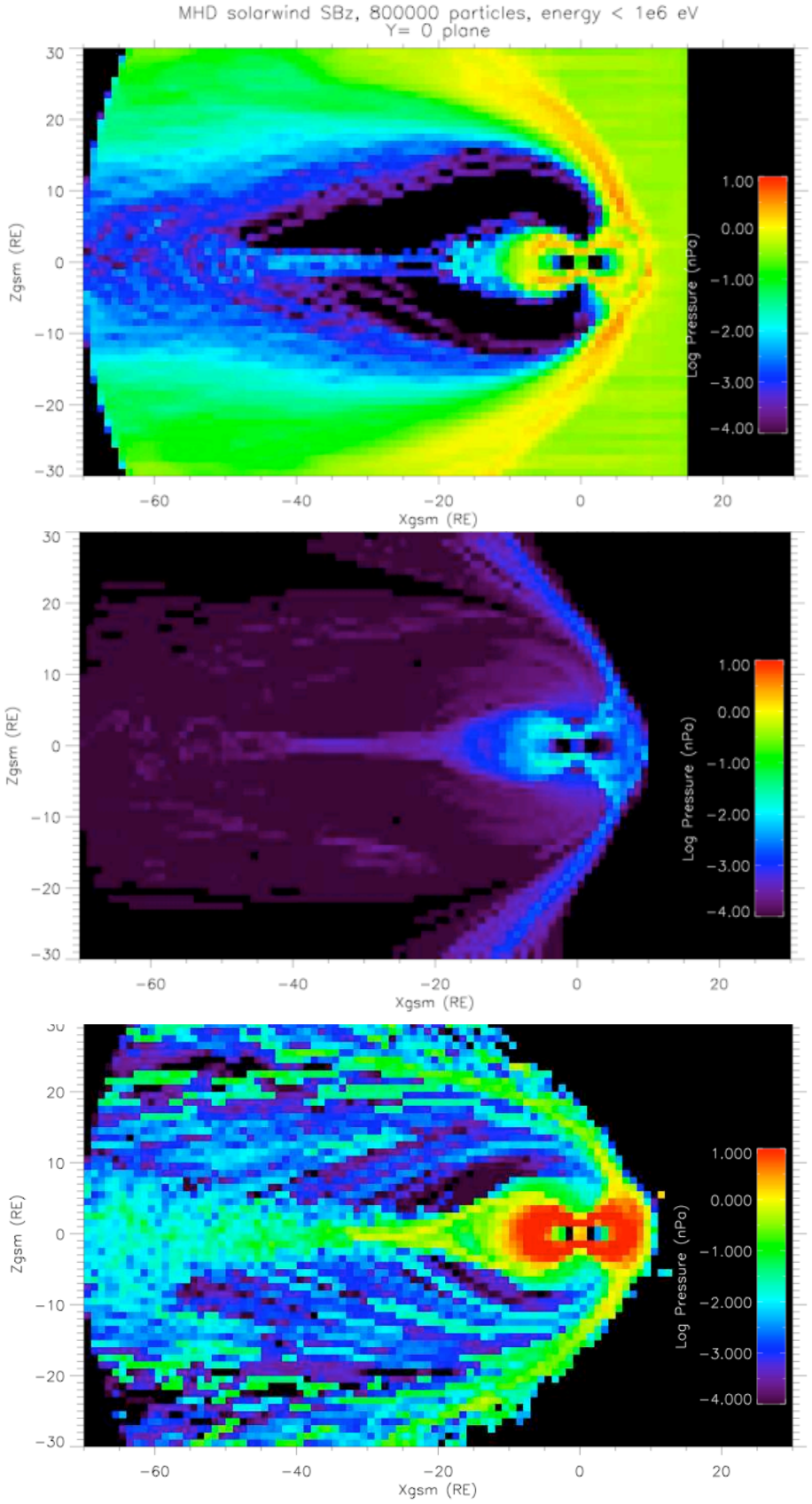
MHD solarwind SBz, 800000 particles, energy < 1e6 eV
Y= 0 plane
Zgsm (RE)
Xgsm (RE)
Log Pressure (nPa)
1.00
0.00
-1.00
-2.00
-3.00
-4.00
MHD solarwind SBz, 800000 particles, energy < 1e6 eV
Y= 0 plane
Zgsm (RE)
Xgsm (RE)
Log Pressure (nPa)
1.00
0.00
-1.00
-2.00
-3.00
-4.00
MHD solarwind SBz, 800000 particles, energy < 1e6 eV
Y= 0 plane
Zgsm (RE)
Xgsm (RE)
Log Pressure (nPa)
1.000
0.000
-1.000
-2.000
-3.000
-4.000

Figure 6

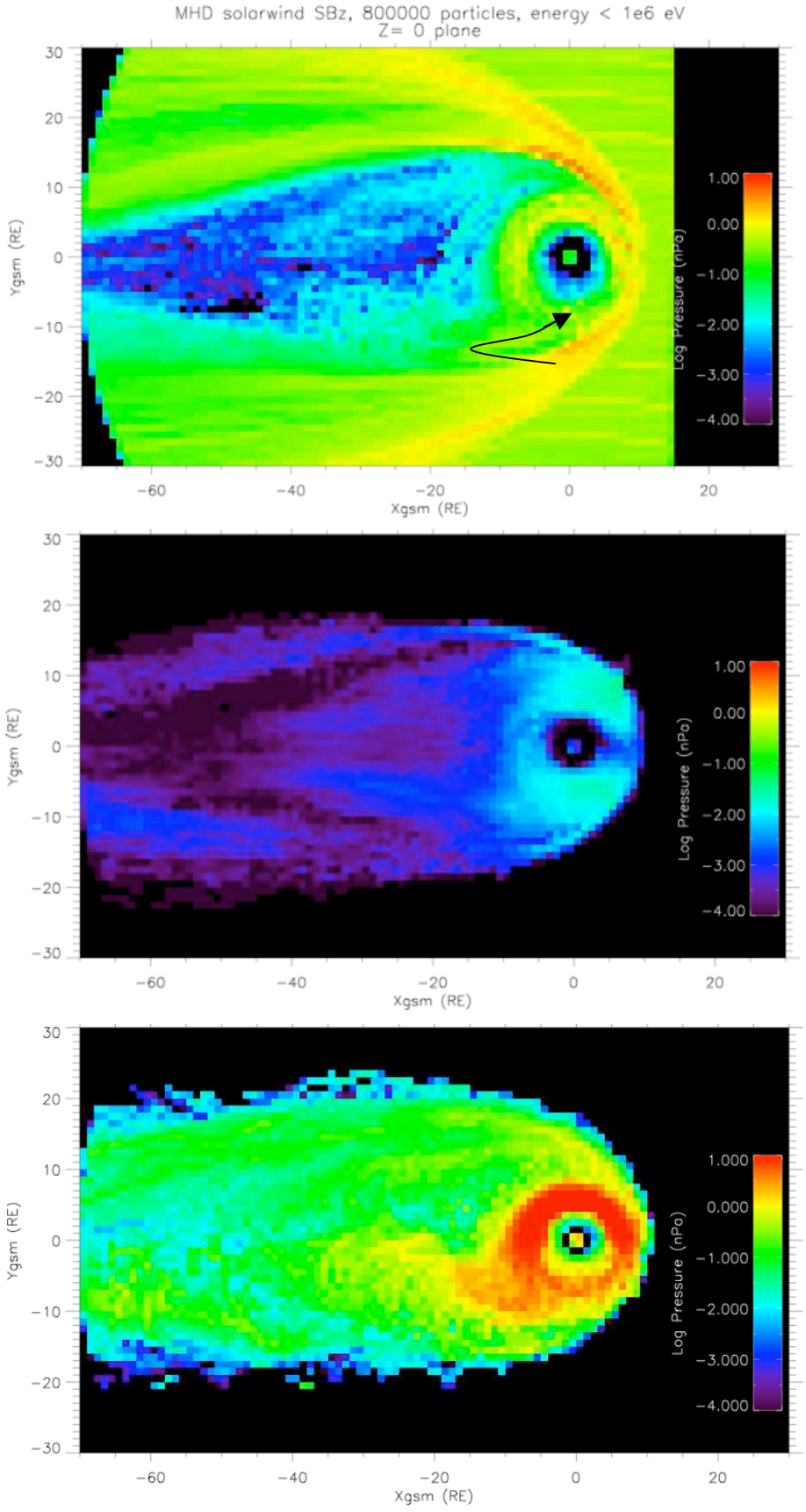
MHD solarwind SBz, 800000 particles, energy < 1e6 eV
Z= 0 plane
Ygsm (RE)
Xgsm (RE)
Log Pressure (nPa)
1.00
0.00
-1.00
-2.00
-3.00
-4.00
1.000
0.000
-1.000
-2.000
-3.000
-4.000

Figure 7

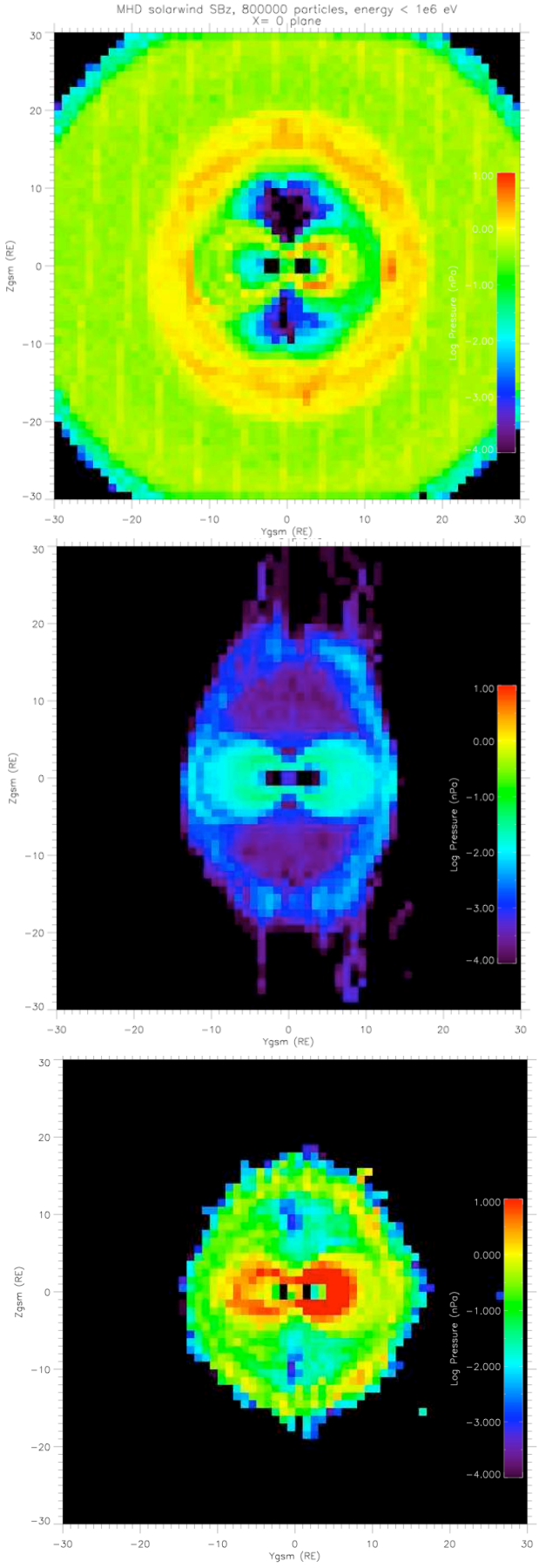
MHD solarwind SBz, 800000 particles, energy < 1e6 eV
X= 0 plane
Zgsm (RE)
Ygsm (RE)
Log Pressure (nPa)
1.00
0.00
-1.00
-2.00
-3.00
-4.00
MHD solarwind SBz, 800000 particles, energy < 1e6 eV
X= -10 plane
Zgsm (RE)
Ygsm (RE)
Log Pressure (nPa)
1.00
0.00
-1.00
-2.00
-3.00
-4.00
MHD solarwind SBz, 800000 particles, energy < 1e6 eV
X= -20 plane
Zgsm (RE)
Ygsm (RE)
Log Pressure (nPa)
1.000
0.000
-1.000
-2.000
-3.000
-4.000

Figure 8

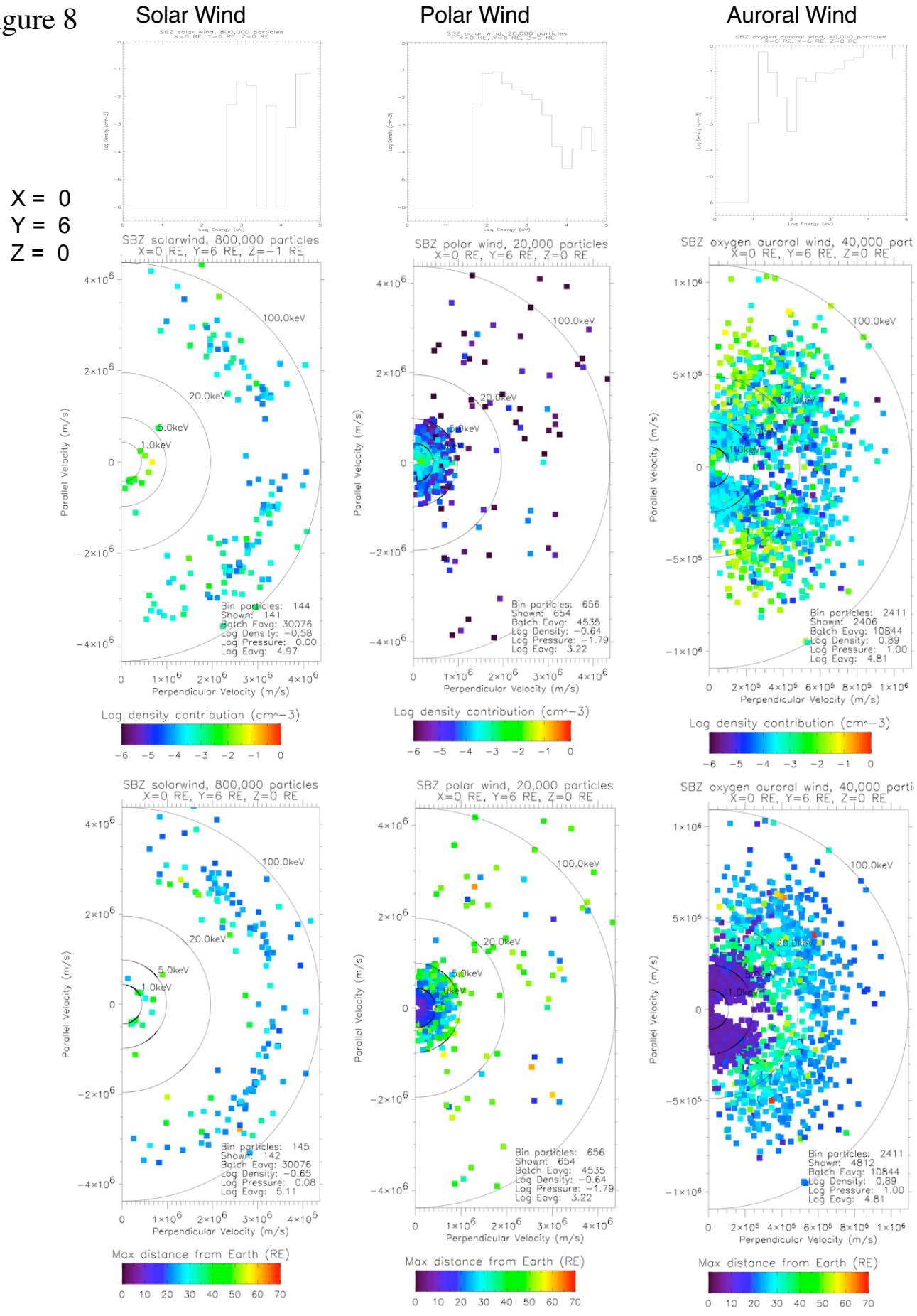
Solar Wind
Polar Wind
Auroral Wind
X = 0
Y = 6
Z = 0
SBZ solarwind, 800,000 particles
X=0 RE, Y=6 RE, Z=−1 RE
SBZ polar wind, 20,000 particles
X=0 RE, Y=6 RE, Z=0 RE
SBZ oxygen auroral wind, 40,000 part
X=0 RE, Y=6 RE, Z=0 RE
100.0keV
20.0keV
5.0keV
1.0keV
Parallel Velocity (m/s)
Perpendicular Velocity (m/s)
Bin particles: 144
Shown: 141
Batch Eavg: 30076
Log Density: −0.58
Log Pressure: 0.00
Log Eavg: 4.97
Bin particles: 656
Shown: 654
Batch Eavg: 4535
Log Density: −0.64
Log Pressure: −1.79
Log Eavg: 3.22
Bin particles: 2411
Shown: 2406
Batch Eavg: 10844
Log Density: 0.89
Log Pressure: 1.00
Log Eavg: 4.81
Log density contribution (cm^−3)
SBZ solarwind, 800,000 particles
X=0 RE, Y=6 RE, Z=0 RE
SBZ polar wind, 20,000 particles
X=0 RE, Y=6 RE, Z=0 RE
SBZ oxygen auroral wind, 40,000 parti
X=0 RE, Y=6 RE, Z=0 RE
Bin particles: 145
Shown: 142
Batch Eavg: 30076
Log Density: −0.65
Log Pressure: 0.08
Log Eavg: 5.11
Bin particles: 656
Shown: 654
Batch Eavg: 4535
Log Density: −0.64
Log Pressure: −1.79
Log Eavg: 3.22
Bin particles: 2411
Shown: 4812
Batch Eavg: 10844
Log Density: 0.89
Log Pressure: 1.00
Log Eavg: 4.81
Max distance from Earth (RE)

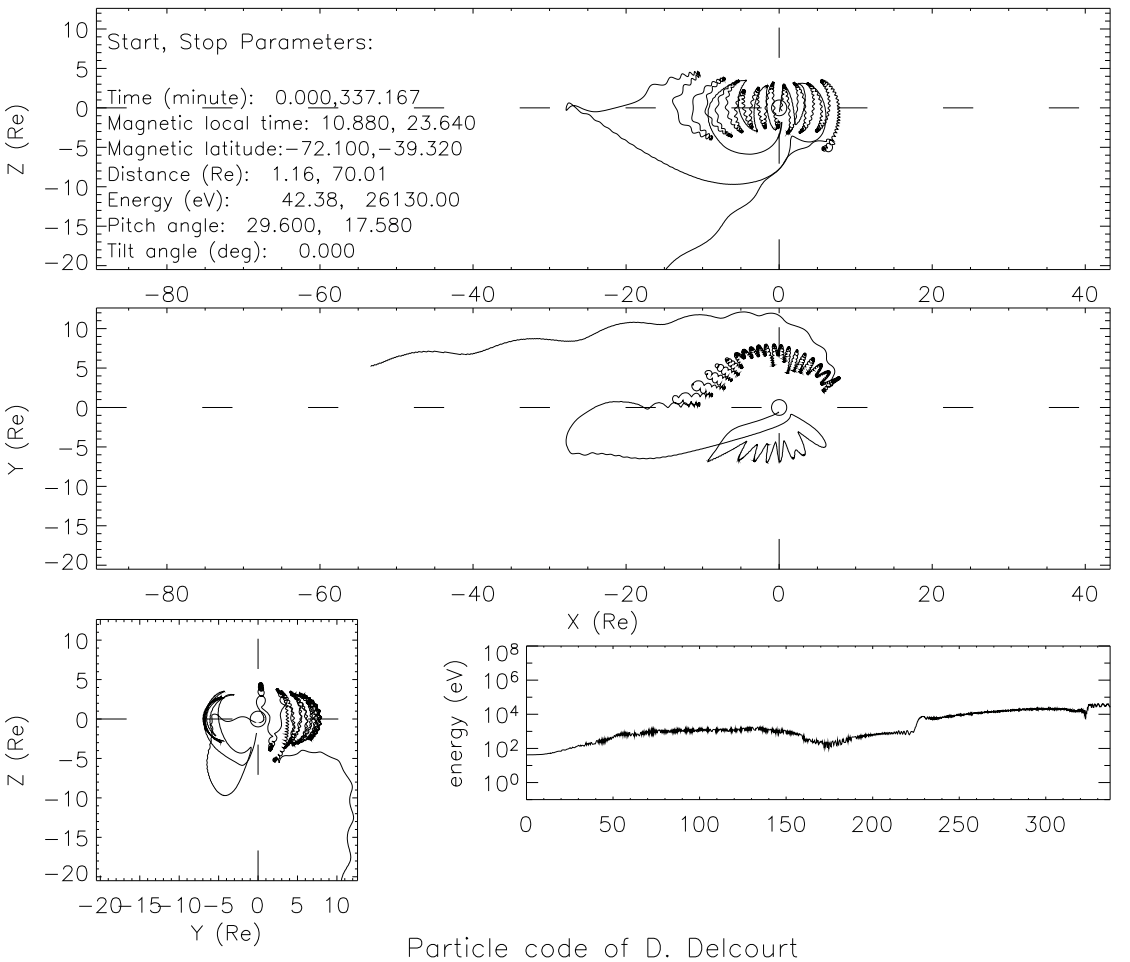
Particle code of D. Delcourt
Start, Stop Parameters:
Time (minute): 0.000,337.167
Magnetic local time: 10.880, 23.640
Magnetic latitude:−72.100,−39.320
Distance (Re): 1.16, 70.01
Energy (eV): 42.38, 26130.00
Pitch angle: 29.600, 17.580
Tilt angle (deg): 0.000
Z (Re)
Y (Re)
X (Re)
energy (eV)

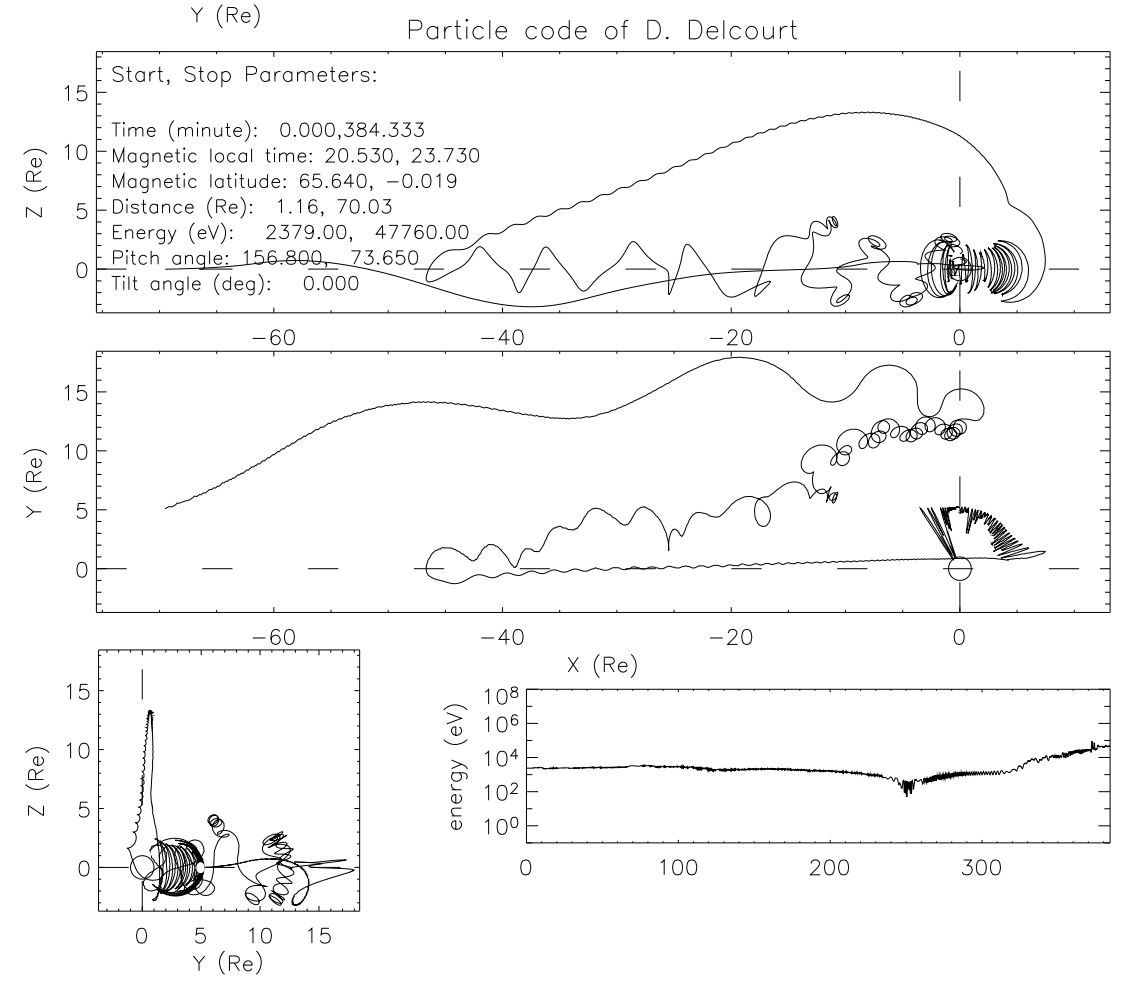
Particle code of D. Delcourt
Start, Stop Parameters:
Time (minute): 0.000,384.333
Magnetic local time: 20.530, 23.730
Magnetic latitude: 65.640, −0.019
Distance (Re): 1.16, 70.03
Energy (eV): 2379.00, 47760.00
Pitch angle: 156.800, 73.650
Tilt angle (deg): 0.000
Z (Re)
Y (Re)
X (Re)
energy (eV)